In Situ High Selectivity Contact-Electroreduction of CO_2 to Methanol Using an Imine-Mediated Metal-Free Vitrimer Catalyst

Nannan Wang[1‡], Haisong Feng[2‡], Jing Yang[3‡], Jie Zheng[1*], Yong-Wei Zhang[3], Nikos Hadjichristidis[4*], Zibiao Li[1,5*]

[1] Institute of Sustainability for Chemicals, Energy and Environment (ISCE[2]), Agency for Science, Technology and Research (A*STAR), 1 Pesek Road, Jurong Island, Singapore 627833, Republic of Singapore;

[2] State Key Laboratory of Chemical Resource Engineering, Beijing Advanced Innovation Center for Soft Matter Science and Engineering, Beijing University of Chemical Technology, Beijing 100029, P. R. China;

[3] Institute of High-Performance Computing (IHPC), A*STAR, 1 Fusionopolis Way, #16-16 Connexis, Singapore 138632, Republic of Singapore;

[4] Polymer Synthesis Laboratory, Chemistry Program, KAUST Catalysis Center, Physical Sciences and Engineering Division, King Abdullah University of Science and Technology (KAUST), Thuwal, 23955, Saudi Arabia;

[5] Institute of Materials Research and Engineering (IMRE), A*STAR, 2 Fusionopolis Way, Innovis #08-03, Singapore 138634, Republic of Singapore;

*Corresponding author. Email: Zheng_Jie@isce2.a-star.edu.sg; Nikolaos.Hadjichristidis@kaust.edu.sa; lizb@imre.a-star.edu.sg;

‡ These authors contributed equally to this work

Abstract

Metal catalysts for the CO_2 reduction reaction (CO_2RR) face challenges such as high cost, limited durability and environmental impact. Although various structurally diverse and functional metal-free catalysts have been developed, they often suffer from slow kinetics, low selectivity, and non-recyclability, significantly limiting their practical applications. In this study, we introduce a recyclable non-metallic polymer material (vitrimer) as a catalyst for a new platform in contact-electro-catalysis. This approach

harnesses the contact charges generated between water droplets and vitrimer to drive CO_2RR, achieving methanol selectivity exceeding 90%. The imine groups within the vitrimer play a dual role, facilitating CO_2 adsorption and enriching friction-generated electrons, thereby mediating efficient electron transfer between the imine groups and CO_2 to promote CO_2RR. After 84 h of CO_2RR, the system achieved a methanol production rate of 13 $nmol \cdot h^{-1}$, demonstrating the excellent stability of the method. Moreover, the vitrimer retains its high-performance electrocatalytic activity even after recycling. Mechanistic studies reveal that, compared to traditional metal catalysts, the N-O bond in the imine, which adsorbs the key intermediate $*OCH_3$, breaks more readily to produce methanol, resulting in enhanced product selectivity and yield. This efficient and environmentally friendly contact-electroreduction strategy for CO_2 offers a promising pathway toward a circular carbon economy by leveraging natural water droplet-based contact-electrochemistry.

Keywords: Contact-electrocatalysis; CO_2 reduction; Metal-free catalyst; vitrimer; High-selectivity

1. Introduction

The conversion of CO_2 into value-added chemicals and fuels represents one of the most promising strategies to address pressing energy and environmental challenges[1-3]. In recent years, extensive studies have focused on reducing CO_2 into various products using advanced electrocatalysis, photocatalysis, and piezocatalysis methods. Notably, electrochemical reduction of CO_2 powered by renewable sources, such as triboelectricity generated through mechanical energy, offers a potential pathway for CO_2 transformation under mild conditions[4-5]. Unlike traditional electrocatalysis, which requires the formation of an electric current loop, the contact-electrocatalytic process relies on the electrostatic charges (electrons) generated by friction to directly participate in the catalytic process *in situ*, eliminating the need for a conductive catalyst. Among the possible products, alcohols with high energy density, particularly methanol, are

highly desirable[6-8]. As a vital platform molecule in the chemical industry, methanol holds significant potential as a direct, clean fuel. However, the electroreduction of CO_2 to methanol presents inherent challenges due to the complex six-electron transfer pathway and slow kinetics involved[9]. Additionally, hybrid structures' interfacial complexity and thermodynamic instability often lead metal-based catalysts to suffer from low selectivity, poor durability, and susceptibility to gas poisoning and environmental degradation[10]. Combined with the high cost and scarcity of precious metals, these challenges hinder the large-scale commercialization of metal-based catalysts in renewable energy technologies. Consequently, developing low-cost, efficient alternatives to metal-based catalysts is imperative for advancing sustainable energy solutions.

Metal-free catalysts have gained increasing attention as efficient electrocatalysts for CO_2RR due to their low cost and high catalytic activity, demonstrating electrocatalytic performance that rivals that of precious metal catalysts[11-13]. However, despite these advancements, the synthesis process of non-metal catalysts remains highly complex. Moreover, their CO_2RR performance is still largely constrained by slow kinetics, high overpotentials, and lower selectivity compared to their metal-based counterparts. A critical limitation of most non-metallic catalysts, such as carbon nanotubes (CNTs), covalent organic frameworks (COFs), and hexagonal boron nitride (h-BN), is their non-recyclability. The disposal of these materials as waste poses severe environmental risks, potentially creating new ecological challenges in the effort to mitigate CO_2 pollution. Furthermore, the high costs associated with managing this waste add an additional layer of complexity to the widespread adoption of non-metallic catalysts.

Due to the strong electron affinity of the C=N bond, imine-based metal-free catalysts facilitate efficient CO_2 adsorption and promote the formation of key reduction intermediates, such as *COOH and *CO. These properties have made imine-based electrocatalysts a prominent focus of research efforts[14-15]. Furthermore, imine bonds exhibit dynamic characteristics through imine exchange or metathesis reactions, enabling the development of Covalent Adaptable Networks (CANs). CANs, which

feature rearrangeable topologies, represent a new class of materials that bridge the gap between high-strength, durable thermosets and flexible, reprocessable thermoplastics, garnering increasing attention in recent years[16-17]. Within the realm of CANs, "vitrimers" have emerged as a standout innovation, utilizing an associative bond exchange mechanism[18]. This mechanism preserves a consistent crosslinking density during processing, ensuring excellent dimensional stability and enhanced material properties.[19-20]. However, imine-based vitrimers often rely on active nucleophilic amino groups or catalysts, which can trigger undesirable side reactions and compromise performance. To address these challenges, we recently introduced a novel metathesis reaction between C=C and C=N bonds to fabricate high-performance vitrimers[21]. This innovative approach offers several advantages over traditional imine exchange or metathesis reactions, including higher efficiency, catalyst-free operation, and exceptional moisture resistance. These features position the C=C/C=N metathesis reaction as a groundbreaking tool to advance vitrimer technology and unlock new possibilities in the design of next-generation materials.

Herein, we propose, for the first time the use of a covalent adaptable network (i.e., vitrimer) featuring both C=C and C=N bonds as a non-metal catalyst for *in situ* solid-liquid contact-electrocatalytic CO_2RR to produce methanol. The strong adsorption capability of the imine bonds within the vitrimer stabilizes the adsorption configuration of CO_2, thereby lowering its activation energy and promoting the formation of the *COOH intermediate. Furthermore, the imine groups effectively enrich frictional charges (electrons) generated by the impact of water droplets on vitrimer and mediate the electron transfer from C=N bond to CO_2, further facilitating the formation of reaction intermediates. This synergy enhances both the efficiency and selectivity of CO_2 conversion. The results demonstrate that the contact-electrocatalytic CO_2RR sustains catalysis for up to 84 h with remarkable stability, achieving a methanol production rate of 13 $nmol \cdot h^{-1}$ and an outstanding selectivity exceeding 90%. Moreover, the presence of both C=C and C=N bonds within the polymer network enables excellent recyclability through the C=C/C=N metathesis reaction. More importantly, the methanol production

rate from the vitrimer-based contact-electrocatalytic CO_2RR remains virtually unchanged before and after recycling, demonstrating the reliability of this method and its promising potential for practical applications. This vitrimer-based contact-electroreduction strategy, utilizing natural water droplets, not only offers a viable pathway for methanol production but also opens new avenues for designing advanced catalysts that combine high performance, recyclability, and environmental compatibility.

2. Results and Discussion

2.1 Preparation and characteristics of the CCCN-vitrimer

To investigate the dynamic behavior between C=C and C=N bonds, Knoevenagel (Kn) compounds (Kn1 and Kn2) incorporating C=C bonds, along with aldimines containing C=N bonds (A1 and A2), were synthesized (**Figures S1–S4**). As shown in **Figure S5**, four compounds (Kn1, Kn2, A1, and A2) with similar intensity were observed within 12 h after mixing Kn1 and A2 in DMSO-d_6 (0.2 M), indicating reversible exchange. A similar equilibrium was observed with Kn2 and A1 as reactants (**Figure S5**). To gain further insight, we conducted kinetic studies by reacting Kn1 and A2 in equal amounts and monitoring the reaction *in situ* via ^{1}H NMR under mild, catalyst-free conditions (rt, air). As shown in **Figure S6**, the product peaks (Kn2 and A1) appeared immediately, reaching equilibrium after ~10 h with ~50% conversion of Kn1 and A2 to Kn2 and A1. Building on this model reaction, we investigated the dynamic properties of a vitrimer containing C=C/C=N bonds (CCCN-vitrimer). The CCCN-vitrimer was prepared by mixing commercially available terephthalaldehyde (TPA), tris(2-aminoethyl) amine (TAA), and a bifunctional crosslinker (2AC, **Figure S7**) in a one-pot, catalyst-free process (**Figure 1a**). The FTIR spectra of the monomers (2AC, TPA, and TAA) and the CCCN-vitrimer are shown in **Figure 1b**. Compared to the monomers, the FTIR spectrum of CCCN-vitrimer exhibits two distinct absorption peaks at approximately 1601 cm^{-1} and 1639 cm^{-1}, corresponding to the C=C and C=N bonds, respectively, confirming the formation of the crosslinked network containing these bonds.

To further validate the formation of the crosslinked polymer, we conducted swelling tests on CCCN-vitrimer in various solvents, including dimethylformamide (DMF), dichloromethane (DCM), tetrahydrofuran (THF), acetonitrile (ACN), ethanol (EtOH), and H_2O. The CCCN-vitrimer network demonstrated high stability, exhibiting low swelling ratios in solvents such as DCM (28%), ACN (11%), and EtOH (5%), indicative of a highly crosslinked structure (**Figure 1c** and **S8**). Additionally, gel content analysis in these solvents (DMF, DCM, THF, ACN, EtOH, and H_2O) revealed high gel content (≥95%) across all samples (**Figure 1c**), further supporting the formation of the crosslinked network.

As shown in **Figure S9**, the initial decomposition temperature ($T_{5\%}$, temperature at 5% weight loss) of CCCN-vitrimer is approximately 270°C, indicating excellent thermal stability. The glass transition temperature (T_g) of CCCN-vitrimer was found to be 98°C as determined by differential scanning calorimetry (DSC) (**Figure S10**), slightly lower than the 136°C obtained by dynamic mechanical analysis (DMA) (**Figure S11**), due to differences in measurement techniques. The storage modulus of CCCN-vitrimer as a function of temperature shows a high value of 1445 MPa below T_g (136°C) and a robust rubbery plateau of 35.06 MPa above T_g, indicating a well-defined crosslinked structure (**Figure S11**). The crosslinking density (ρ) of the polymer network was calculated to be 3127 mol m^{-3}. Such a high crosslinking density imparts increased rigidity and enhanced dimensional stability, making the material exceptionally durable and well-suited for real-world applications.

Due to the presence of both C=C and C=N bonds within the polymer network, the resulting CCCN-vitrimer exhibits a rearrangeable topology through C=C/C=N metathesis (**Figure 1d**). The dynamic feature of C=C/C=N exchange within the polymer network was analyzed via stress relaxation at elevated temperatures (190°C, 200°C, 210°C, and 220°C) using DMA. As shown in **Figure 1e** the stress relaxation moduli decreased exponentially over time, indicating that the crosslinked polymer behaves as a vitrimer, capable of stress relaxation over extended periods due to the dynamic C=C/C=N exchange reaction. The relaxation time (τ*), defined as the time

required to relax 1/e (36.7%) of the initial stress, was determined using the Maxwell model for viscoelastic fluids. With increasing temperature, the exchange rate accelerated, and τ* decreased from 3.16 minutes at 190°C to 1.34 minutes at 220°C. According to Arrhenius' law, the activation energy (E_a) for the C=C/C=N exchange reaction in CCCN-vitrimer was calculated to be 55 kJ mol^{-1} (**Figure 1f)**, consistent with results for other materials containing C=C/C=N bonds[21]. Thanks to these dynamic C=C/C=N linkages, CCCN-vitrimer exhibits efficient reprocessing capabilities. After mechanical failure, the CCCN-vitrimer sample was cut into small pieces and hot-pressed at 180°C and 30 bar for 30 min, completely restoring the polymer network (**Figure 1g**). The recycled CCCN-vitrimer retained its surface properties, as evidenced by contact angle measurements of 93.93° before recycling and 94.23° after recycling (**Figure S12**). Furthermore, FTIR analysis confirmed that no significant structural changes occurred during reprocessing (**Figure 13**).

Given that imine-modified catalysts are commonly used to enhance CO_2 adsorption (**Table S1**), the primary role of introducing C=N groups into the vitrimer is to increase CO_2 adsorption capacity, thereby facilitating the subsequent contact electroreduction of CO_2. We then characterized the CO_2 adsorption capacity of CCCN-vitrimer with varying C=N bond content, as shown in **Figure 1h**. Based on the ratio of C=C to C=N bonds, CCCN-vitrimers with different imine contents were prepared and designated as $V_{2\text{-}1}$, $V_{1\text{-}1}$, and $V_{1\text{-}2}$ in order of increasing imine content. A control polymer without C=N bonds was also synthesized and designated polymer-CC (**Figures S14** and **S15**). The results indicate that CO_2 adsorption increases with higher C=N content, demonstrating that the incorporation of imine groups effectively enhances the CO_2 capture capacity of CCCN-vitrimer. Importantly, imine groups selectively adsorb CO_2, while their adsorption of N_2 remains very weak (**Figure 1i**), highlighting the practical applicability of imine-functionalized vitrimers for CO_2 capture under real-world conditions. To further investigate CO_2 adsorption, DFT calculations were performed to determine the binding energies of CO_2 and N_2 with the vitrimer. The results revealed that the adsorption energy between CCCN-vitrimer and CO_2 molecules is 0.44 eV (**Figure 1j**),

while for N_2 is 0.21 eV (**Figure 1k**). These findings confirm that CO_2 is preferentially and more readily adsorbed onto the CCCN-vitrimer molecules, consistent with the experimental results.

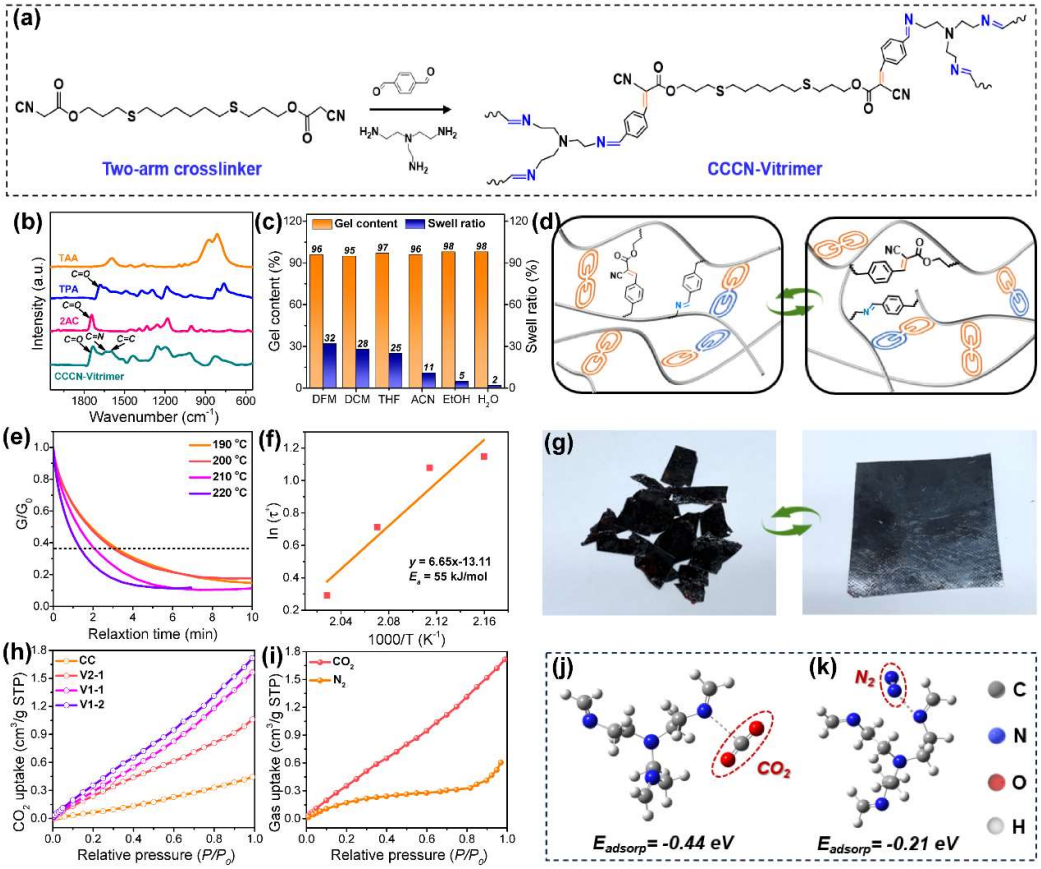

Figure 1. Preparation and characteristics of the CCCN-vitrimer. (a) Schematic illustration of the preparation of vitrimer containing C=C and C=N bonds (CCCN-vitrimer). (b) IR spectra of polymer monomers (TPA, TAA, and 2AC) and CCCN-vitrimer. (c) Swelling ratio and gel content of CCCN-vitrimer in various solvents. (d) Schematic illustration of the dynamic structure of the vitrimer network showing recyclability. (e) Stress relaxation curves of CCCN-vitrimer at different temperatures. (f) Fitting of the relaxation time to the Arrhenius equation. (g) Photographs illustrating the recycling process of CCCN-vitrimer. (h) CO_2-BET of vitrimers with different imine contents and imine-free polymer (CC). (i) CO_2- and N_2-BET of CCCN-vitrimer. (j, k) Comparison of the adsorption energies of CO_2 and N_2 on CCCN-vitrimer.

2.2 Device and catalytic process for contact-electroreduction of CO_2

Building on the aforementioned foundational study, we incorporated the prepared CCCN-vitrimer into a solid-liquid contact electrification system to develop a metal-free contact-electroreduction of CO_2 device. The schematic of the device used for methanol production via contact-electroreduction of CO_2 is shown in **Figure 2a**. Inside a 2.5 L sealed box, a 45-degree inclined plane coated with the vitrimer is positioned 30 cm below the water inlet. Adjacent to the water inlet is a CO_2 inlet, which also serves as the outlet for CO_2 gas products. A reservoir at the bottom of the chamber collects methanol as the primary liquid product. During operation, the generated methanol is enriched through circulation using a small peristaltic pump, allowing for more precise measurement of product yield. A photograph of the complete setup is provided in **Figure S16**. To visualize the charge distribution generated during contact between water droplets and the CCCN-vitrimer, we observed the spreading process of water droplets on the vitrimer surface and measured its surface potential. **Figure 2b** shows sequential high-speed camera images of a water droplet spreading across the CCCN-vitrimer surface, illustrating rapid dispersion within 19 ms. It is noteworthy that due to the presence of imine groups, the surface of vitrimer exhibits hydrophobic properties[22], with a contact angle of approximately 94° (**Figure S12**). As a result, water droplets in contact with the vitrimer will quickly slide off the surface, exhibiting a rapid contact-separation dynamic behavior, which leads to the generation of triboelectricity[23]. We then used a Kelvin probe to test the surface potential distribution of the CCCN-vitrimer, as shown in **Figure 2c**. Due to the accumulation effect of triboelectric charges, the surface potential of CCCN-vitrimer increases with the number of droplet impacts. Furthermore, since water is a common triboelectrically positive material[24], the water droplets become positively charged upon triboelectrification. These positively charged droplets subsequently catalyze water oxidation, producing protons that participate in the CO_2 reduction reaction (CO_2RR).

We then calculated the electron distribution of the CCCN-vitrimer, as shown in **Figure 2d**. The results indicate that electrons are primarily concentrated on the imine groups,

confirming the electron-rich effect induced by the presence of C=N bonds. Furthermore, in designing the vitrimer molecules, we intentionally introduced electron-withdrawing functional groups, such as cyano and carbonyl groups, to enhance the triboelectric properties of the vitrimer[25-26]. The roles of these functional groups withinin the CCCN-vitrimer molecules are illustrated in **Figure S17**. To summarize, during the triboelectrification process with water droplets, the presence of cyano, carbonyl, and imine groups on the CCCN-vitrimer membrane surface generates a large amount of frictional negative charge (electrons), which then accumulate around the imine groups. Given the high affinity of C=N bonds for CO_2 adsorption, when CO_2 interacts with the CCCN-vitrimer, electron transfer occurs from the C=N bonds to the CO_2 molecules. To verify the electron transfer mechanism between CO_2 and the CCCN-vitrimer upon contact, we conducted DFT calculations to analyze the charge distribution near the CCCN-vitrimer surface, as shown in **Figure 2e**. When the distance between the CO_2 molecule and the C=N bond exceeds 5 Å, no significant interaction is observed between the charges of CO_2 and the nitrogen atom. However, as the distance decreases to 4 Å, electron accumulation occurs between the carbon atom of CO_2 and the nitrogen atom of the C=N bond. This accumulation intensifies as the CO_2 molecule moves closer to the nitrogen atom, leading to a significant build-up of electrons. Consequently, when CO_2 comes into contact with the C=N bond, electrons can rapidly transfer from the nitrogen atom to the CO_2 molecule. To illustrate the catalytic process, we present a macroscopic schematic of the reaction mechanism following the impact of a water droplet on the CCCN-vitrimer in the presence of CO_2 (**Figure 2f)**. First, CO_2 is adsorbed onto the C=N groups (**Figure 2f i**). Then, as a water droplet contacts the CCCN-vitrimer, triboelectric charging occurs, causing the CCCN-vitrimer to become negatively charged while the water molecules acquire a positive charge (**Figure 2f ii**). Positive charges in the water drive oxidation reactions, producing protons that participate in the CO_2RR. Simultaneously, electrons in the CCCN-vitrimer are transferred to the adsorbed CO_2, initiating a reduction reaction (**Figure 2f iii**). Finally, as the water droplet slides off the surface, the electrons in the CCCN-vitrimer continue

to facilitate CO_2RR, enabling the reaction to proceed continuously (**Figure 2f iv**).

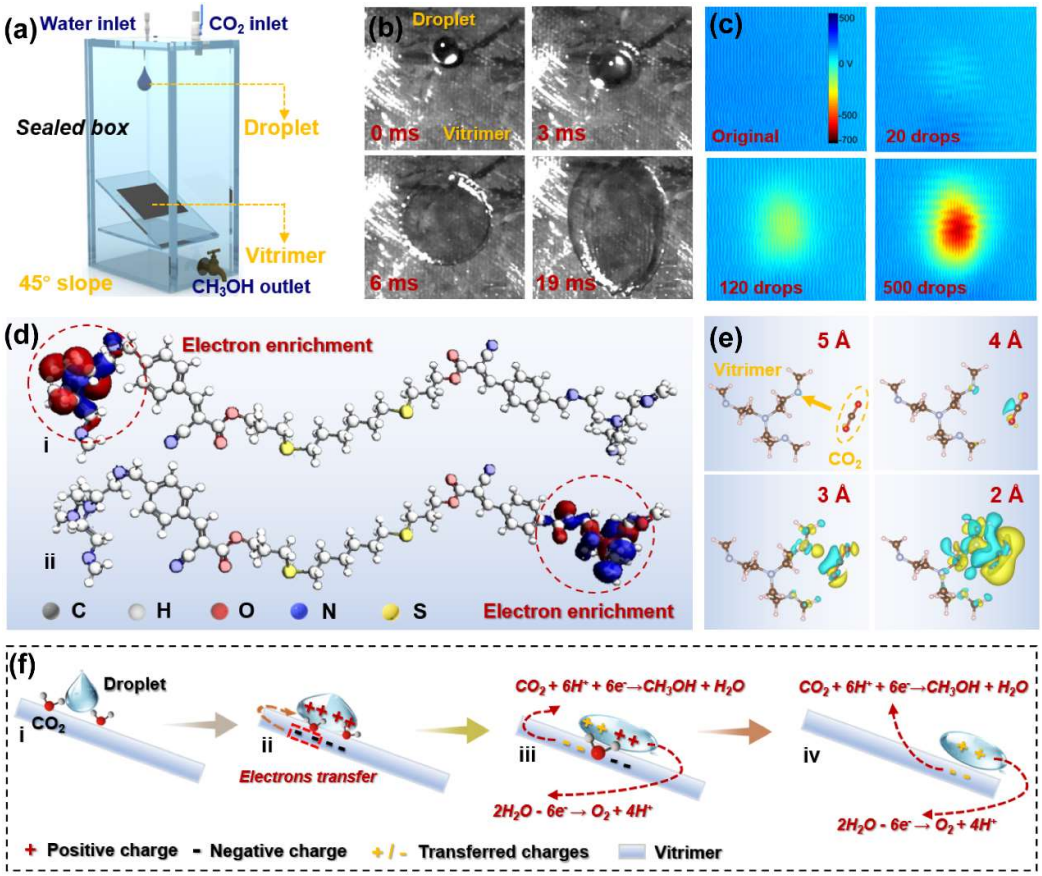

Figure 2. Device and catalytic process for the contact-electroreduction of CO_2. (a) Schematic diagram of the contact-electrocatalytic device for methanol production. (b) Dynamic optical image showing the water droplets spreading on the vitrimer surface. (c) Effect of water droplet impact number on surface potential distribution. (d) Electron distribution of the conduction band edge in the CCCN-vitrimer. (e) Charge distribution during the contact between CO_2 molecules and vitrimer. (f) Schematic representation of the integrated charge generation and consumption process in the water droplet–vitrimer contact-electrocatalytic CO_2RR.

2.3 Performance of contact-electroreduction of CO_2

We subsequently investigated the performance of CO_2 electroreduction upon contact between water droplets and the CCCN-vitrimer. Before testing, the CCCN-vitrimer was purged with N_2 for 1 hour on a heating plate at 110 °C to activate the C=N sites. The

CCCN-vitrimer was then attached to the inclined plate of a sealed chamber, where water droplets impacted the surface at a frequency of 1 Hz for 5 h. A small peristaltic pump was used to circulate the resulting aqueous solution, enriching the methanol concentration. Product samples were collected every hour and analyzed by ^{1}H-NMR, with dimethyl sulfoxide (DMSO) as an internal standard and D_2O as solvents. The results confirm the appearance of methanol at 3.2 ppm in the ^{1}H-NMR spectrum, with the peak area increasing with reaction time (**Figure 3a** and the inset). The variation in methanol production over 5 hours is shown in **Figure 3b**, while the inset illustrates the increase in CO production over time. Additionally, the CO yield, calculated based on GC analysis, is summarized in **Table S2**. The calculated methanol selectivity is approximately 91%. To evaluate the effect of C=N content on methanol yield during contact-electroreduction of CO_2, vitrimers with varying imine contents (CC, $V_{2\text{-}1}$, $V_{1\text{-}1}$ and $V_{1\text{-}2}$) were tested. The results show that the methanol yield from the CCCN-vitrimers containing C=N is significantly higher than that from the C=N-free polymer CC, indicating that the introduction of C=N enhances the contact electrocatalytic CO_2RR. Furthermore, the methanol yield of $V_{1\text{-}2}$ with a lower C=N content is significantly lower than that of $V_{1\text{-}1}$ with a higher C=N content, further confirming that the presence of the C=N bond is essential for methanol production. In additional, $V_{1\text{-}1}$ produced slightly higher methanol yields than $V_{1\text{-}2}$. This could be attributed to phase separation in $V_{1\text{-}2}$, caused by excessive C=N content (inset of **Figure 3c**), which reduces triboelectric efficiency and CO_2 adsorption performance. To assess the recyclability of the CCCN-vitrimer, $V_{1\text{-}1}$ was used as the study subject, and its methanol yield was compared before and after recycling (**Figure 3d**). The results demonstrate only a minimal change in methanol yield after recycling, confirming the excellent reusability of the CCCN-vitrimer and its potential for practical applications.

To determine the origin of methanol and CO in the products, isotopically pure $^{13}CO_2$ gas was used as the source in the solid-liquid contact electroreduction of CO_2, and the products were analyzed by ^{1}H-NMR and GC-MS. When using $^{13}CO_2$ instead of CO_2, the ^{1}H NMR spectrum of the reaction solution in **Figure 3e** shows a doublet between

3.56 and 3.04 ppm, attributed to the protons coupled with ^{13}C in $^{13}CH_3OH$[27]. This result directly indicates that CO_2 serves as the carbon source for the solid-liquid contact electrocatalytic reduction of CO_2 to CH_3OH. Furthermore, the source of CO was investigated using GC-MS. To enhance the detection sensitivity of the target compound, the selective ion monitoring (SIM) mode was employed to detect the presence of ^{13}CO (m/z = 29) in the mixed gas. The mass spectrum (**Figure 3f**) reveals three main peaks for CO with the strongest signal at m/z = 29 corresponding to ^{13}CO, and two additional fragments at m/z = 13 (^{13}C) and m/z = 16 (O). The GC spectrum of gaseous products from contact electroreduction of CO_2 using $^{13}CO_2$ as the carbon source is shown in **Figure S18**. These findings clearly indicate that CO originates from contact electrocatalytic CO_2RR. Furthermore, to demonstrate its excellent water resistance, CCCN-vitrimer underwent a 7-day soaking test, as shown in **Figure S19**. The results show that after 7 days, the CCCN-vitrimer retained its surface morphology and flexibility, confirming its excellent water resistance and suitability as a durable solid-liquid triboelectric layer material for real-world applications. Based on this, an 84-hour cyclic experiment was conducted to evaluate the stability of the solid-liquid contact-electroreduction of CO_2 to methanol. Liquid products were recirculated using a peristaltic pump to enrich methanol, with samples collected every 12 hour for analysis via ^{1}H-NMR and GC. The results show that the ^{1}H-NMR spectra of methanol over 84 h show a gradual increase in the peak area of methanol without the appearance of impurity peaks (**Figure 3g**), demonstrating the excellent stability of this method. Furthermore, after continuous operation for 84 hours, the methanol yield remained at approximately 13 nmol·h^{-1} (**Figure 3h**), indicating that the CCCN-vitrimer surface can continuously provide electrons for CO_2RR under water droplet impact, achieving a selectivity for methanol exceeding 90%.

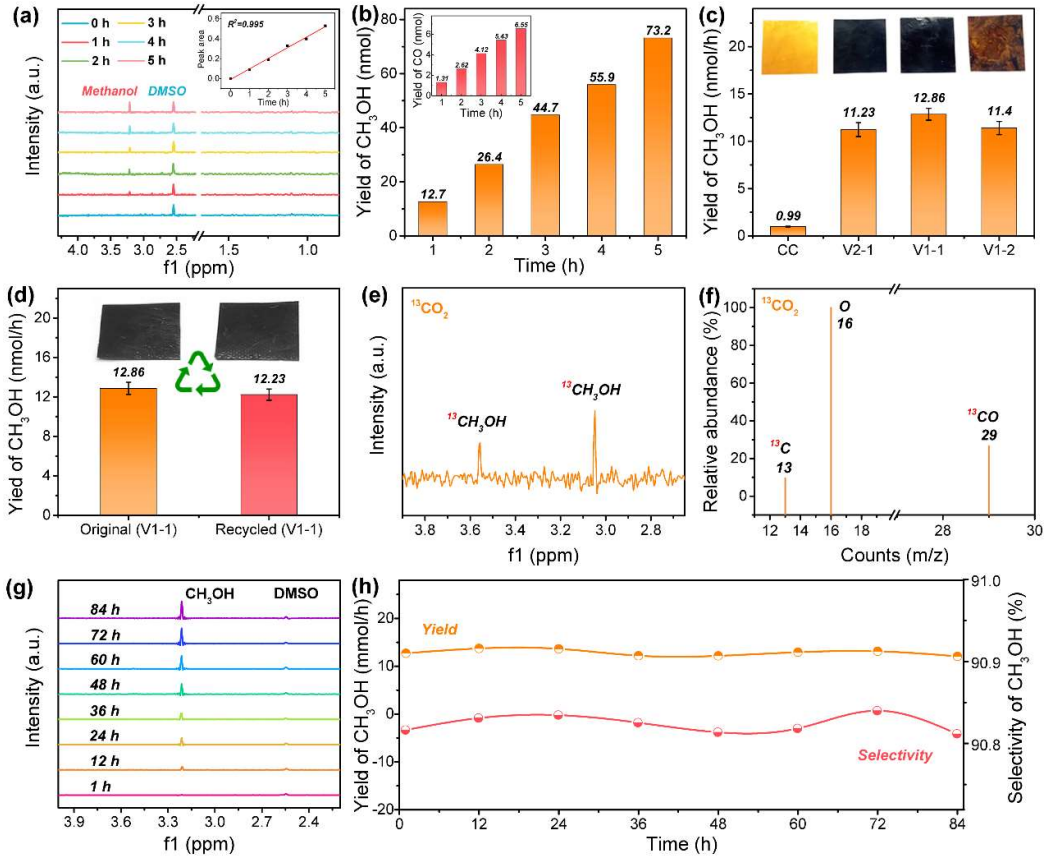

Figure 3. Performance of contact-electroreduction of CO_2. (a) ^{1}H-NMR spectra of the products from solid-liquid contact-electrocatalytic CO_2RR. The inset shows the methanol peak area obtained based on the integration relative to the internal standard. (b) Variation in methanol yield over time. The inset shows the corresponding variation in CO yield. (c) Comparison of methanol yields in contact-electrocatalytic CO_2 reduction using CCCN-vitrimers with different C=N bond contents and the CC-polymer without C=N bonds. The inset shows optical photographs of these membranes. (d) Comparison of methanol yields in contact-electrocatalytic CO_2 reduction using CCCN-vitrimer before and after recycling. (e) ^{1}H-NMR spectra of the contact-electro-catalytic reaction solution using labeled $^{13}CO_2$. (f) GC-MS of CO in the isotope experiment with $^{13}CO_2$. **(g, h)** ^{1}H-NMR, methanol yield, and selectivity for CO_2RR via contact electrocatalysis during 84-hour cyclic operation.

2.4 Mechanism of contact-electroreduction of CO_2 to methanol

Based on the performance analysis of contact electrocatalytic CO_2 reduction to

methanol, density functional theory DFT calculations were employed to explore the underlying mechanism of CO_2RR. As shown in **Figure 4a**, CO_2 preferentially adsorbs onto the nitrogen site of the C=N bond in the initial activation step. At this site, the formation of *COOH can achieve a stable configuration with relatively low free energy (0.55 eV), indicating that imine plays a synergistic role in facilitating CO_2 activation. After *COOH is formed and subsequently reduced to *CO, the *CHO intermediate is generated. Due to the strong interaction between *CHO and the nitrogen atom, this step is exothermic. Subsequently, *CHO is adsorbed and further accepts electrons and protons to form *OCH_2 and *OCH_3, which are ultimately reduced to methanol. We found that the formation of *CH_2O into *CH_3O is highly endothermic and likely serves as the rate-determining step (RDS), as this step requires the highest energy barrier (0.92 eV). Overall, these findings suggest that the presence of an imine functionality significantly enhances the electrocatalytic reduction of $CO_2$to methanol.

From a molecular perspective, compared to traditional metal catalysts (e.g., Cu), the pathway for electrochemical CO_2RR to methanol is common and involves the adsorption of the key reaction intermediate *OCH_3 on a Cu atom (metal catalyst) or an N atom (metal-free catalyst), forming Cu-*OCH_3 or N-*OCH_3. Subsequently, the Cu-O or N-O bond cleaves to produce *OCH_3, as shown in **Figure S20**. To understand the high selectivity of the non-metal catalyst in contact-electrocatalytic CO_2 reduction to methanol, we used *OCH3 as a probe to calculate the bond dissociation energies (ΔE) of Cu-O or N-O bond cleavage in the metal catalyst (Cu) and the non-metal catalyst (CCCN-vitrimer). The results show that on Cu (111), the cleavage of the Cu-O bond is an endothermic reaction, with a calculated $\Delta E_{Cu\text{-}O}$ value of 0.57 eV (**Figure 4b**). In contrast, on the nitrogen atom of the C=N bond, the cleavage of the N-O bond is an exothermic reaction, with a calculated $\Delta E_{N\text{-}O}$ value of -1.98 eV. This indicates that the cleavage of the N-O bond on the non-metal catalyst CCCN-vitrimer is more favorable for releasing *OCH_3, leading to a significant difference in methanol selectivity between the two catalysts. Therefore, based on catalytic performance, spectroscopic characterization, and DFT calculations, we propose a possible catalytic mechanism for

the solid-liquid contact-electrocatalytic reduction of CO_2 to methanol on the non-metallic CCCN-vitrimer catalyst (**Figure 4c)**. In the CCCN-vitrimer molecule, the C=N bonds in the imine effectively capture and activate gaseous CO_2. Simultaneously, contact electrification between CCCN-vitrimer and water molecules leads to the oxidation of H_2O, generating protons. In aqueous solution, these protons readily transfer to $*CO_2$, and, with the assistance of electrons, sequentially hydrogenate to form the $*OCH_3$ intermediate. Because the cleavage of the N-O bond in C=N-$*OCH_3$ is exothermic (spontaneous), methanol is ultimately produced as the final product through subsequent hydrogenation steps.

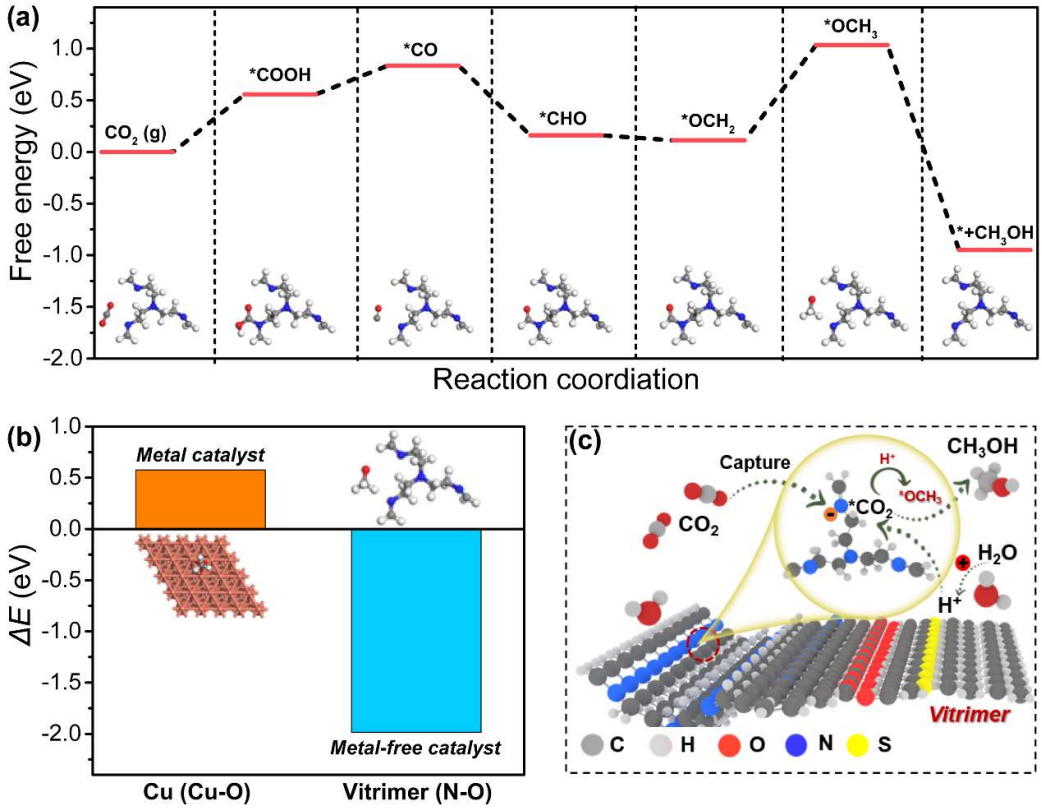

Figure 4. Theoretical calculations on the contact-electroreduction of CO_2 to methanol mechanism. (a) Free-energy diagrams of the methanol formation pathway on CCCN-vitrimer. (b) Calculated ΔH values for Cu-O and N-C bonds in the Cu-$*OCH_3$ and N-$*OCH_3$ intermediates on Cu (111) and CCCN-vitrimer, respectively. (c) Proposed synergetic mechanism for methanol formation from CO_2 during the contact electrification of water droplets with CCCN-vitrimer, mediated by imine bonds.

3. Conclusion

In conclusion, we have delineated a novel pathway for CO_2 reduction to methanol that differs from traditional electrocatalysis. This approach uses a vitrimer-based, metal-free catalyst containing imine groups to catalyze CO_2 reduction to methanol through static electricity generated by solid-liquid contact electrification, achieving an exceptionally high selectivity of 91%. The mechanism relies on the dual functionality of the imine bonds within the vitrimer, which not only provides excellent CO_2 adsorption capacity but also creates an electron-rich environment that facilitates the contact-electrocatalytic CO_2RR process. Additionally, compared to traditional metal catalysts, the N–O bond formed on the imine sites, which absorbs the key intermediate *OCH_3 intermediate, is more readily cleaved to release methanol, thereby enhancing both product selectivity and yield. More importantly, the vitrimer catalyst exhibits excellent recyclability through C=C/C=N metathesis reactions, maintaining an essentially unchanged methanol production rate after multiple cycles. This reliability underscores its potential for practical applications. Overall, this sustainable and metal-free strategy offers significant advantages over conventional catalytic methods, providing a promising pathway toward efficient methanol production and advancing CO_2 utilization technologies.

ASSOCIATED CONTENT

Data Availability Statement

The data described in this paper are available from the corresponding authors upon reasonable request.

Supporting Information

The Supporting Information is available free of charge on the ACS Publications website. It includes details on materials and characterization methods, synthesis and experimental procedures, characterization data including ^{1}H-NMR spectrum,

Thermogravimetric analysis (TGA), Kinetics of bond dynamic exchange, Infrared spectrum (IR), Contact angle and Gas chromatography (GC).

AUTHOR INFORMATION

Corresponding Authors

Jie Zheng—Institute of Sustainability for Chemicals, Energy and Environment ($ISCE^2$), Agency for Science, Technology and Research (A*STAR), 1 Pesek Road, Jurong Island, Singapore 627833, Republic of Singapore; orcid.org/ 0000-0003-4859-0671; Email: Zheng_Jie@isce2.a-star.edu.sg.

Nikos Hadjichristidis—Polymer Synthesis Laboratory, Chemistry Program, KAUST Catalysis Center, Physical Sciences and Engineering Division, King Abdullah University of Science and Technology (KAUST), Thuwal 23955, Saudi Arabia*; orcid.org/0000-0003-1442-1714;Email: mailto:nikolaos.hadjichristidis@kaust.edu.sa.*

Zibiao Li—Institute of Sustainability for Chemicals, Energy and Environment ($ISCE^2$), Agency for Science, Technology and Research (A*STAR), 1 Pesek Road, Jurong Island, Singapore 627833, Republic of Singapore; orcid.org/0000-0002-0591-5328; Email: lizb@imre.a-star.edu.sg.

Authors

Nannan Wang—Institute of Sustainability for Chemicals, Energy and Environment ($ISCE^2$), Agency for Science, Technology and Research (A*STAR), 1 Pesek Road, Jurong Island, Singapore 627833, Republic of Singapore.

Haisong Feng—State Key Laboratory of Chemical Resource Engineering, Beijing Advanced Innovation Center for Soft Matter Science and Engineering, Beijing University of Chemical Technology, Beijing 100029, P. R. China.

Jing Yang—Institute of High Performance Computing (IHPC), Agency for Science, Technology and Research (A*STAR), 1 Fusionopolis Way, #16-16 Connexis, Singapore 138632, Republic of Singapore.

Yong-Wei Zhang—Institute of High Performance Computing (IHPC), Agency for Science, Technology and Research (A*STAR), 1 Fusionopolis Way, #16-16 Connexis,

Singapore 138632, Republic of Singapore.

Notes

The authors declare no competing financial interest.

ACKNOWLEDGMENTS

This project is supported by the Agency for Science, Technology and Research (A*STAR) under RIE2025 the Manufacturing, Trade and Connectivity (MTC) Programmatic Funding (Grant No. M22K9b0049) and Science and Engineering Research Council (SERC) Central Research Fund (Use-inspired Basic Research). J. Yang and Y. Zhang would like to acknowledge the funding support from the Italy-Singapore Science and Technology Cooperation (Grant No. R23101R040). The use of computing resources at the A*STAR Computational Centre and National Supercomputer Centre, Singapore, is gratefully acknowledged. N. H. gratefully acknowledges the support of King Abdullah University of Science and Technology (KAUST).

References

1. Gao, W.; Xu, Y.; Fu, L.; Chang, X.; Xu, B., Experimental evidence of distinct sites for CO_2-to-CO and CO conversion on Cu in the electrochemical CO_2 reduction reaction. *Nat. Catal.* **2023,** *6* (10), 885-894.
2. Okatenko, V.; Loiudice, A.; Newton, M. A.; Stoian, D. C.; Blokhina, A.; Chen, A. N.; Rossi, K.; Buonsanti, R., Alloying as a strategy to boost the stability of copper nanocatalysts during the electrochemical CO_2 reduction reaction. *J. Am. Chem. Soc.* **2023,** *145* (9), 5370-5383.
3. Wang, C.; Lv, Z.; Yang, W.; Feng, X.; Wang, B., A rational design of functional porous frameworks for electrocatalytic CO_2 reduction reaction. *Chem. Soc. Rev.* **2023,** *52* (4), 1382-1427.
4. Wang, N.; Jiang, W.; Yang, J.; Feng, H.; Zheng, Y.; Wang, S.; Li, B.; Heng, J. Z. X.; Ong, W. C.; Tan, H. R., Contact-electro-catalytic CO_2 reduction from ambient air.

Nat. Commun. **2024,** *15* (1), 5913.

5. Kim, D. H.; Kim, J. K.; Choi, S. Y.; Yang, Y.; Song, H. C.; Park, H. S.; Shim, M.; Baik, J. M., Addressing Triboelectric Nanogenerator Impedance for Efficient CO_2 Utilization. *Adv. Energy Mater.* **2024,** *14* (8), 2304012.
6. Ding, J.; Tang, Q.; Fu, Y.; Zhang, Y.; Hu, J.; Li, T.; Zhong, Q.; Fan, M.; Kung, H. H., Core–shell covalently linked graphitic carbon nitride–melamine–resorcinol–formaldehyde microsphere polymers for efficient photocatalytic CO_2 reduction to methanol. *J. Am. Chem. Soc.* **2022,** *144* (22), 9576-9585.
7. Navarro-Jaén, S.; Virginie, M.; Bonin, J.; Robert, M.; Wojcieszak, R.; Khodakov, A. Y., Highlights and challenges in the selective reduction of carbon dioxide to methanol. *Nat. Rev. Chem.* **2021,** *5* (8), 564-579.
8. Bagchi, D.; Raj, J.; Singh, A. K.; Cherevotan, A.; Roy, S.; Manoj, K. S.; Vinod, C.; Peter, S. C., Structure-tailored surface oxide on Cu–Ga intermetallics enhances CO_2 reduction selectivity to methanol at ultralow potential. *Adv. Mater.* **2022,** *34* (19), 2109426.
9. Yang, P.-P.; Gao, M.-R., Enrichment of reactants and intermediates for electrocatalytic CO_2 reduction. *Chem. Soc. Rev.* **2023,** *52* (13), 4343-4380.
10. Pei, C.; Chen, S.; Fu, D.; Zhao, Z.-J.; Gong, J., Structured Catalysts and Catalytic Processes: Transport and Reaction Perspectives. *Chem. Rev.* **2024,** *124* (6), 2955-3012.
11. Ghausi, M. A.; Xie, J.; Li, Q.; Wang, X.; Yang, R.; Wu, M.; Wang, Y.; Dai, L., CO_2 Overall Splitting by a Bifunctional Metal-Free Electrocatalyst. *Angew. Chem., Int. Ed.* **2018,** *57* (40), 13135-13139.
12. Zhang, B.; Zhang, J.; Zhang, F.; Zheng, L.; Mo, G.; Han, B.; Yang, G., Selenium-doped hierarchically porous carbon nanosheets as an efficient metal-free electrocatalyst for CO_2 reduction. *Adv. Funct. Mater.* **2020,** *30* (3), 1906194.
13. Mohata, S.; Das, R.; Koner, K.; Riyaz, M.; Das, K.; Chakraborty, S.; Ogaeri, Y.; Nishiyama, Y.; C Peter, S.; Banerjee, R., Selective metal-free CO_2 photoreduction in water using porous nanostructures with internal molecular free volume. *J. Am.*

Chem. Soc. **2023,** *145* (43), 23802-23813.

14. Liu, Q.; Yang, X.; Li, L.; Miao, S.; Li, Y.; Li, Y.; Wang, X.; Huang, Y.; Zhang, T., Direct catalytic hydrogenation of CO_2 to formate over a Schiff-base-mediated gold nanocatalyst. *Nat. commun.* **2017,** *8* (1), 1407.
15. Dong, Y.-L.; Liu, H.-R.; Wang, S.-M.; Guan, G.-W.; Yang, Q.-Y., Immobilizing isatin-schiff base complexes in NH2-UiO-66 for highly photocatalytic CO_2 reduction. *ACS Catal.* **2023,** *13* (4), 2547-2554.
16. Scheutz, G. M.; Lessard, J. J.; Sims, M. B.; Sumerlin, B. S., Adaptable crosslinks in polymeric materials: resolving the intersection of thermoplastics and thermosets. *J. Am. Chem. Soc.* **2019,** *141* (41), 16181-16196.
17. Fan, X.; Zheng, J.; Yeo, J. C. C.; Wang, S.; Li, K.; Muiruri, J. K.; Hadjichristidis, N.; Li, Z., Dynamic Covalent Bonds Enabled Carbon Fiber Reinforced Polymers Recyclability and Material Circularity. *Angew. Chem.* **2024,** *136* (40), e202408969.
18. Denissen, W.; Winne, J. M.; Du Prez, F. E., Vitrimers: permanent organic networks with glass-like fluidity. *Chem. Sci.* **2016,** *7* (1), 30-38.
19. Wang, S.; Ma, S.; Li, Q.; Xu, X.; Wang, B.; Huang, K.; Liu, Y.; Zhu, J., Facile preparation of polyimine vitrimers with enhanced creep resistance and thermal and mechanical properties via metal coordination. *Macromolecules* **2020,** *53* (8), 2919-2931.
20. Zhang, S.; Yi, J.; Chen, J.; Li, Y.; Liu, B.; Lu, Z., Weldable, Reprocessable, and Water-resistant Polybenzoxazine Vitrimer Crosslinked by Dynamic Imine Bonds. *ChemSusChem* **2024**, e202301708.
21. Zheng, J.; Feng, H.; Zhang, X.; Zheng, J.; Ng, J. K. W.; Wang, S.; Hadjichristidis, N.; Li, Z., Advancing Recyclable Thermosets through C═ C/C═ N Dynamic Covalent Metathesis Chemistry. *J. Am. Chem. Soc.* **2024,** *146* (31), 21612-21622.
22. Mohd, N. K.; Kian, Y. S.; Ibrahim, N. A.; Nor, S. M. M.; Wan Yunus, W. M. Z.; Ghazali, M. J.; Huei, L. W., Corrosion inhibition, adsorption and thermodynamic properties of hydrophobic-tailed imines on carbon steel in hydrochloric acid solution: a comparative study. *J. Adhes. Sci. Technol.* **2021,** *35* (23), 2558-2579.

23. Lin, S.; Chen, X.; Wang, Z. L., Contact electrification at the liquid–solid interface. *Chem. Rev.* **2021,** *122* (5), 5209-5232.
24. Nie, J.; Ren, Z.; Xu, L.; Lin, S.; Zhan, F.; Chen, X.; Wang, Z. L., Probing contact-electrification-induced electron and ion transfers at a liquid–solid interface. *Adv. Mater.* **2020,** *32* (2), 1905696.
25. Dixon, D. A.; Eades, R. A.; Frey, R.; Gassman, P. G.; Hendewerk, M. L.; Paddon-Row, M. N.; Houk, K., Theoretical evaluation of the effect of electron-withdrawing substituents on carbocation stabilities. Delocalization of charge to the carbonyl and cyano groups. *J. Am. Chem. Soc.* **1984,** *106* (14), 3885-3891.
26. Wang, N.; Liu, Y.; Ye, E.; Li, Z.; Wang, D., Control methods and applications of interface contact electrification of triboelectric nanogenerators: a review. *Mater. Res. Lett.* **2022,** *10* (3), 97-123.
27. Bin Yeo, J.; Ho Jang, J.; In Jo, Y.; Woo Koo, J.; Tae Nam, K., Paired Electrosynthesis of Formaldehyde Derivatives from CO_2 Reduction and Methanol Oxidation. *Angew. Chem.* **2024,** *136* (2), e202316020.